MADRID
inter.noise 2019
June 16 - 19
NOISE CONTROL FOR A BETTER ENVIRONMENT

TIME DOMAIN PHASE COHERENCE BASED ALGORITHM FOR IMPACT SOURCE RECONSTRUCTION

Maxime BILODEAU[1], Nicolas QUAEGEBEUR, Olivier ROBIN, Patrick O'DONOUGHUE, Patrice MASSON, and Alain BERRY
Groupe d'Acoustique de l'Université de Sherbrooke
Department of Mechanical Engineering, Sherbrooke, QC, J1K 2R1, Canada

ABSTRACT

The characterization of vibroacoustic sources using microphone arrays in the time domain is still challenging because of the bad conditioning and extensive computational resources required to solve the associated ill-posed problem. The Near-field Acoustical Holography (NAH) framework and the Time-Reversal techniques are among the approaches proposed to solve this problem. However, such techniques involve either dense microphone arrays in the vicinity of the sources to be characterized or high computational complexity. This work proposes a new Time-Domain Phase Coherence algorithm (TD-PCa) based on the phase coherence principle widely used in the fields of image processing and ultrasound imaging. The proposed TD-PCa is numerically and experimentally validated using a regular 121 microphone array located in front of an impacted, baffled, simply-supported plate in an anechoic chamber. The resulting vibration field is reconstructed with the proposed TD-PCa and compared with the vibration field estimated with the Delay-and-Sum (DAS) standard approach. Moreover, the imaging results are compared with vibration field measurements conducted on the plate using the deflectometry technique with a high-speed camera. The results show that the acceleration field reconstructed with the proposed TD-PCa is in good agreement with the vibration field measured optically.

Keywords: Acoustic Imaging, Signal Processing, Phase Coherence
I-INCE Classification of Subject Number: 74
(see http://i-ince.org/files/data/classification.pdf)

[1]Maxime.Bilodeau2@USherbrooke.ca

1. INTRODUCTION

Acoustic source characterization in terms of location and magnitude is a wide branch of engineering acoustics. A complete field of research related to the imaging and characterization of noise sources has emerged in the last decades [1]. While stationary noise sources can be identified with measurements made using a sound intensity probe [2] or a microphone array [3], the identification of transient noise sources is a more challenging problem. It is well known that impacts or squeal noise are common in industrial environments and that they can be harmful to workers. The monitoring of transient noise sources is also of great interest in the transportation industry, where unsteady excitation sources such as turbulent flows are common.

1.1. Acoustic imaging

In order to improve the spatial resolution and dynamic range, as required to accurately characterize multiple point-like noise sources, many approaches based on microphone arrays have been proposed. A recent review paper proposes an objective comparison of the most commonly used techniques [4] throughout a unified formalism. Among the techniques proposed in the literature to reconstruct time varying structural vibration fields, Near-field Acoustical Holography (NAH), Time Reversal (TR) approaches and direct beamforming techniques such as Delay-and-Sum (DAS) are the most widely used. However, NAH methods require dense microphone arrays in the vicinity of the source plane, which can be problematic in several practical situations. Despite the low computational cost of the DAS, this method cannot be used for spatially extended vibration source characterization since velocity reconstruction at a given source point is obtained under the hypothesis that this point behaves as the only radiating point source. Hence, DAS is not suited for extended noise source characterization and is mostly used as a qualitative tool for noise source localization. On the other hand, TR technique potentially requires the use of complex models for simulating wave propagation in the considered acoustic medium [5]. Consequently, the development of an algorithm for the reconstruction of transient sources in the time domain is still relevant and is particularly of interest for the transportation industry.

1.2. Phase coherence

The importance of phase in signals has been recognized and widely used by researchers in optics and image processing. For instance, it is now well known that most of the information from a greyscale image lies in the phase and not in the amplitude of grey levels, contrary to what one would intuitively expect [7]. Although considered for decades in image processing, the idea of mainly exploiting the phase content of the signals was only recently applied in ultrasound imaging. Phase coherence (PC) imaging uses the phase measured by an array of receivers to define a coherence factor ($0 \leq F \leq 1$) that represents the similitude of the phases measured, and thus the likelihood of a source (or reflector) at the considered position [8]. The most employed coherence factors are all defined as functions of the instantaneous phase, its variance and standard deviation calculated among all receivers [8]. Although the concept of instantaneous phase is ambiguous in the time domain, it is well known that steep changes in the phase between subsequent time samples (changes in the sign for instance) carry

much information about the propagation medium. Already used in non-destructive evaluation and in medical imaging, phase coherence imaging is promising for real-time imaging since it allows increasing both the dynamic range and image resolution [9].

In the audible acoustic range, recent work using the generalized cross correlation and steered response power algorithms shows that the use of the Phase Transform (PHAT) results in an increased resolution and in a wider dynamic range. However, when using PHAT filtering, the magnitude of the signals used for absolute sound pressure level reconstruction is lost [10]. Due to their high degree of parallelizability on graphics processor units, these formulations are well suited for real-time imaging [11]. However, the few acoustic imaging algorithms proposed in the literature that use phase filtering have either been developed in the frequency domain, or are not well suited for time domain reconstruction of transient or unsteady events because of the loss of information on the source magnitude [12].

In the present paper, a time domain imaging algorithm that allows for vibration reconstruction of a transient extended source based on the concept of PC is proposed. The proposed algorithm and the framework used throughout the paper are presented in Section 2. In Section 3, a numerical and an experimental validation of the algorithm is proposed for the case of a simply-supported impacted panel. In both cases, the proposed algorithm is compared with the standard DAS method and with the original acceleration field. Experimentally, the acceleration field acting as the reference (ground truth) is reconstructed using a direct optical deflectometry measurement.

2. TIME-DOMAIN PHASE COHERENCE ALGORITHM

As depicted in Figure 1, a regular array of M microphones is positioned at $z = z_m$ above an imaging plane located at $z_0 = 0$. The latter is discretized into N elemental sound radiating elements of identical areas (A_e).

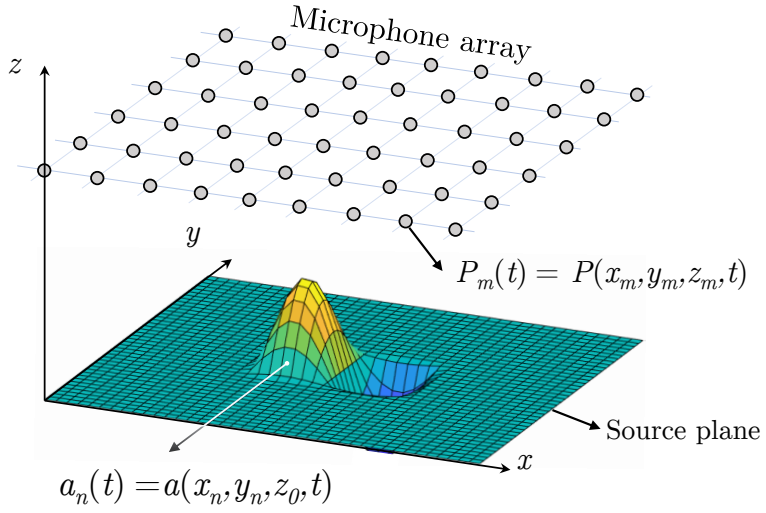

Figure 1: Imaging setup consisting of a regular microphone array to measure the acoustic pressure $P_m(t)$ above an imaging domain that contains a planar acceleration source distribution $a_n(t)$.

Under the hypothesis that the side length of each square element is smaller than half of the smallest structural wavelength considered, each sound radiating element can be seen

as a discrete source monopole. In that case, the measured sound pressure at microphone m can be approximated by :

$$P_m(t) = \rho_o A_e \sum_{n=1}^{N} \frac{\delta(t - R_{mn}/c)}{2\pi R_{mn}} \star a_n(t), \tag{1}$$

where $\star$ is the convolution operator, R_{mn} is the Euclidean distance between microphone m positioned at $[x_m, y_m, z_m]$ and source monopole n positioned at $[x_n, y_n, z_0]$, ρ_0 is the density of the acoustic medium, c is the sound velocity in air and $a_n(t)$ is the normal acceleration of the source monopole n. Before deriving a coherence metric, let us first consider the sole contribution of the pixel n to the sound pressure at microphone m and rewrite it as:

$$\mathbf{P}_{mn} = \frac{\rho_0 A_e}{2\pi} \mathbf{g}_{mn} \mathbf{a}_n \tag{2}$$

where $\mathbf{P}_{mn}$ and $\mathbf{a}_n$ are column time vectors and where $\mathbf{g}_{mn}$ is a real-valued sparse matrix whose non-zero diagonal starts at line $L_{mn} = \lfloor R_{mn}/(c\Delta t) \rceil$ (in which $\lfloor \ldots \rceil$ is the rounding operator and Δt is the inverse of the sampling frequency):

$$\mathbf{g}_{mn} = \frac{1}{R_{mn}} \left[\begin{array}{c|c} 0_{(L_{mn}, K-L_{mn})} & 0_{(L_{mn}, L_{mn})} \\ \hline \mathbb{I}_{(K-L_{mn}, K-L_{mn})} & 0_{(K-L_{mn}, L_{mn})} \end{array} \right] \tag{3}$$

In $\mathbf{g}_{mn}$, 0 and $\mathbb{I}$ denote the null and identity matrices and K is the number of time samples from the first noise event (t_0) to the last measurement on the array (t_{K-1}). The emptiness of the upper part of $\mathbf{g}_{mn}$ is explained by the causality principle. The rounding operator is used to snap the propagation delay R_{mn}/c to the closest discrete time sample. Adding the contribution of all source monopoles contained in the imaging domain to the sound pressure at microphone m and concatenating all (single microphone) linear systems together, one obtains :

$$\mathbf{P} = \frac{\rho_0 A_e}{2\pi} \mathbf{G}\mathbf{A} \tag{4}$$

where $\mathbf{P}$ is a MK vector that denotes the pressure signals at each microphone for the whole time span and $\mathbf{G}$ is a $MK \times NK$ matrix that represents the propagation matrix between the acceleration sources and the sound pressure measurements:

$$\mathbf{P} = \begin{bmatrix} \mathbf{P_1} \\ \vdots \\ \mathbf{P_m} \\ \vdots \\ \mathbf{P_M} \end{bmatrix}; \qquad \mathbf{G} = \begin{bmatrix} \mathbf{G}_1 \\ \vdots \\ \mathbf{G}_m \\ \vdots \\ \mathbf{G}_M \end{bmatrix} = \begin{bmatrix} \mathbf{g}_{11} & \cdots & \mathbf{g}_{1N} \\ \vdots & & \vdots \\ \mathbf{g}_{M1} & \cdots & \mathbf{g}_{MN} \end{bmatrix}; \tag{5}$$

This formalism is sometimes used in NAH where the spatial discretization of the imaging plane coincides well with the spatial discretization of the microphone array, resulting in well-conditioned systems [13]. However, in our case, the under-determination of the linear problem in Equation 4 results in a clearly ill-posed problem. To illustrate this, the case of a time span of 500 samples over a 121 microphone array combined with a 1000 pixel reconstruction grid results in a matrix $\mathbf{G}$ of dimensions [60 500 × 500 000] (i.e. 500 000 unknowns) which requires a system shrinking phase prior to the inversion in order to become solvable. Indeed, the size reduction of $\mathbf{A}$ could help reduce the ill-posedness of Equation 4 and also accelerate the solution computation through the reduction of the

dimensions of **G**. To accomplish this, as for the PC filters used in ultrasound imaging [8], let us define a statistical metric on the instantaneous phase of the M acoustic pressure signals measured at time sample t_i for pixel n:

$$PC(n, t_i) = \left| \frac{1}{M} \sum_{m=1}^{M} \frac{\tilde{P}_m(t_i + R_{mn}/c)}{R_{mn}} \right| \tag{6}$$

where $\tilde{z} = z + jH(z)$ is the analytic representation of $z(n, t)$ in which $j = \sqrt{-1}$ and $H(\cdot)$ is the Hilbert transform operator. This metric calculates the average phasor of the analytical signal over the whole microphone array and its objective is to help identify the pixels that are more likely to contribute to the measured pressure field. Hence, the first step of the proposed time-domain algorithm is to calculate $PC(n, t_i)$ at each time and space sample, and reject from the imaging domain all samples associated to phase coherence values under a given threshold (as schematized in Figure 2).

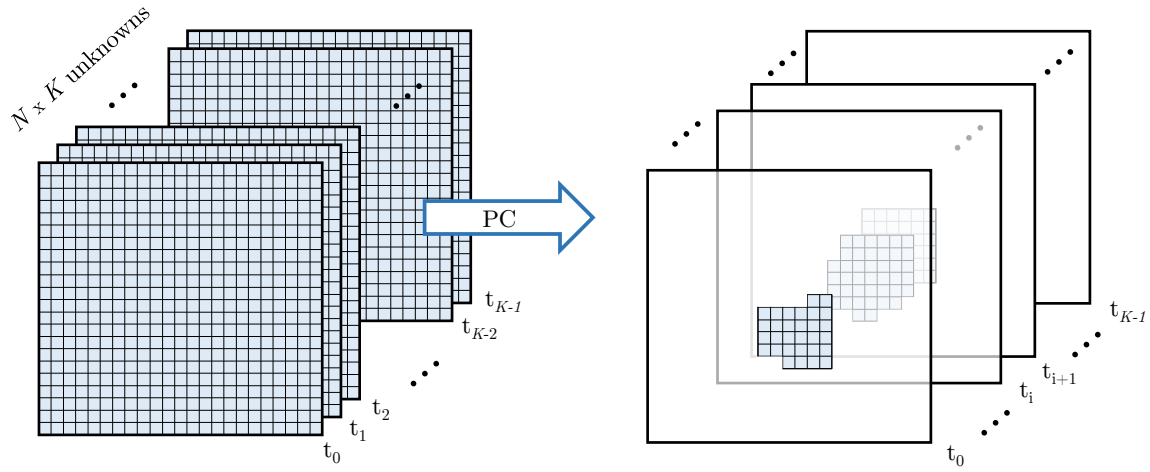

Figure 2: Effect of the PC threshold on the number of pixels considered in the imaging algorithm.

The pixel rejection threshold can take into account many parameters such as the computational power available and *a priori* information about the source (position, dimensions, frequency content, etc.). Following the rejection step, **G** is computed using this new imaging domain and **P** is clipped accordingly (i.e. only the advanced time measurements associated to the kept pixels are used). The resulting system can be solved using various regularization approaches, but the standard Tikhonov regularization is used herein in order to lower the sensitivity of the solution to noise. Using the well-known solution to the Tikhonov regularization, the acceleration of the pixels of interest can be calculated from:

$$\underline{\mathbf{A}}_\lambda = \frac{2\pi}{\rho_0 A_e} \mathbf{G}_\lambda \underline{\mathbf{P}} \tag{7}$$

where $\mathbf{G}_\lambda = (\underline{\mathbf{G}}^H \underline{\mathbf{G}} + \lambda \mathbb{I})^{-1} \underline{\mathbf{G}}^H$, the underline symbol represents the quantity associated to the reduced domain, $(\cdot)^H$ is the conjugate transpose operator and λ is the regularization parameter. For the configurations considered in the present work, the Generalized Cross Validation (GCV) provided slightly better result than the L-curve for the regularization parameter identification and was thus chosen. Hence, the λ value used in Equation 7 is

given by the minimization of [13] :

$$F(\lambda) = \frac{\| \underline{\mathbf{G}}\underline{\mathbf{A}}_{\lambda} - \underline{\mathbf{P}} \|^2}{[\mathrm{Tr}(\mathbb{I} - \underline{\mathbf{G}}^H \underline{\mathbf{G}}_{\lambda}^{-1})]^{-2}} \tag{8}$$

where Tr(.) represents the trace of a matrix. In the present work, the regularization parameter identification and the resolution of Equation 7 is conducted using the *Regularization Tools* MATLAB toolbox [14].

3. ALGORITHM VALIDATION

In order to validate and demonstrate the performance of the Time-Domain Phase Coherence algorithm (TD-PCa) described in Section 2, a baffled simply-supported panel is numerically and experimentally considered. Indeed, referring to Figure 1, a regular square microphone array (11 × 11 microphones) is located at height $z_m = 0.6$ m above the imaging domain into which lies the 3.2 mm thick panel of dimensions: 48 cm × 42 cm. The microphones are separated by $\Delta x = \Delta y = 0.1$ m, resulting in a 1 m × 1 m array with a spatial aliasing frequency of 1 715 Hz. As done in NAH, the imaging domain lying at $z_0 = 0$ has similar dimensions than the microphone array, although using a better refined mesh compared with NAH. The imaging domain is discretized into a grid of 41×41 source monopoles for a total of 1 681 pixels, and 100 time samples at a sampling frequency of 6 400 Hz are considered.

3.1. Numerical Validation

The simulation of the acceleration field of the impacted simply-supported panel is conducted using the modal summation method. Indeed, the vibration response on the whole panel due to a point force at position (x_f, y_f) at a given frequency ω is given by [15]:

$$v(\omega, x, y) = \sum_{\alpha=1}^{\infty} \sum_{\beta=1}^{\infty} u_{\alpha\beta}(\omega)\phi_{\alpha\beta}(x, y), \tag{9}$$

where $u_{\alpha\beta}(\omega)$ and $\phi_{\alpha\beta}$ are the velocity amplitude and mode shape of mode (α,β) respectively, and they are given by :

$$u_{\alpha\beta}(\omega) = \frac{j\omega F \phi_{\alpha\beta}(x_f, y_f)}{[\omega_{\alpha\beta}^2(1 + j\eta) - \omega^2](\rho_s hab/4)}, \quad \phi_{\alpha\beta}(x, y) = \sin\left(\frac{\alpha\pi x}{a}\right)\sin\left(\frac{\beta\pi y}{b}\right). \tag{10}$$

In Equation 10, F is the force amplitude, η is the damping loss factor, ρ_s is the panel density, h is the thickness and a and b are the dimensions of the panel in the x and y directions respectively. In order to find the acceleration field resulting from a point like impact, the modal summation method is used to first construct $v(\omega, x, y)$ frequency by frequency over a wide frequency range. Taking the inverse Fourier transform of the resulting complex velocity field, one obtains the response of the impacted simply supported panel. Following this, the acceleration field of the aluminium panel is obtained with a simple discrete time derivative of the velocity field. The propagation and measurement phases of the simulation are conducted using the time domain acoustic *k-Wave* MATLAB toolbox [16]. Finally, a white noise is added to the simulated sound pressure at each microphone, resulting in a signal to noise ratio of 10 dB.

In order to discuss about the imaging results obtained using TD-PCa, the latter is compared in Figure 3 with the output of the DAS and with the simulated acceleration field (ground truth). In Figure 3, the columns represent three subsequent time samples

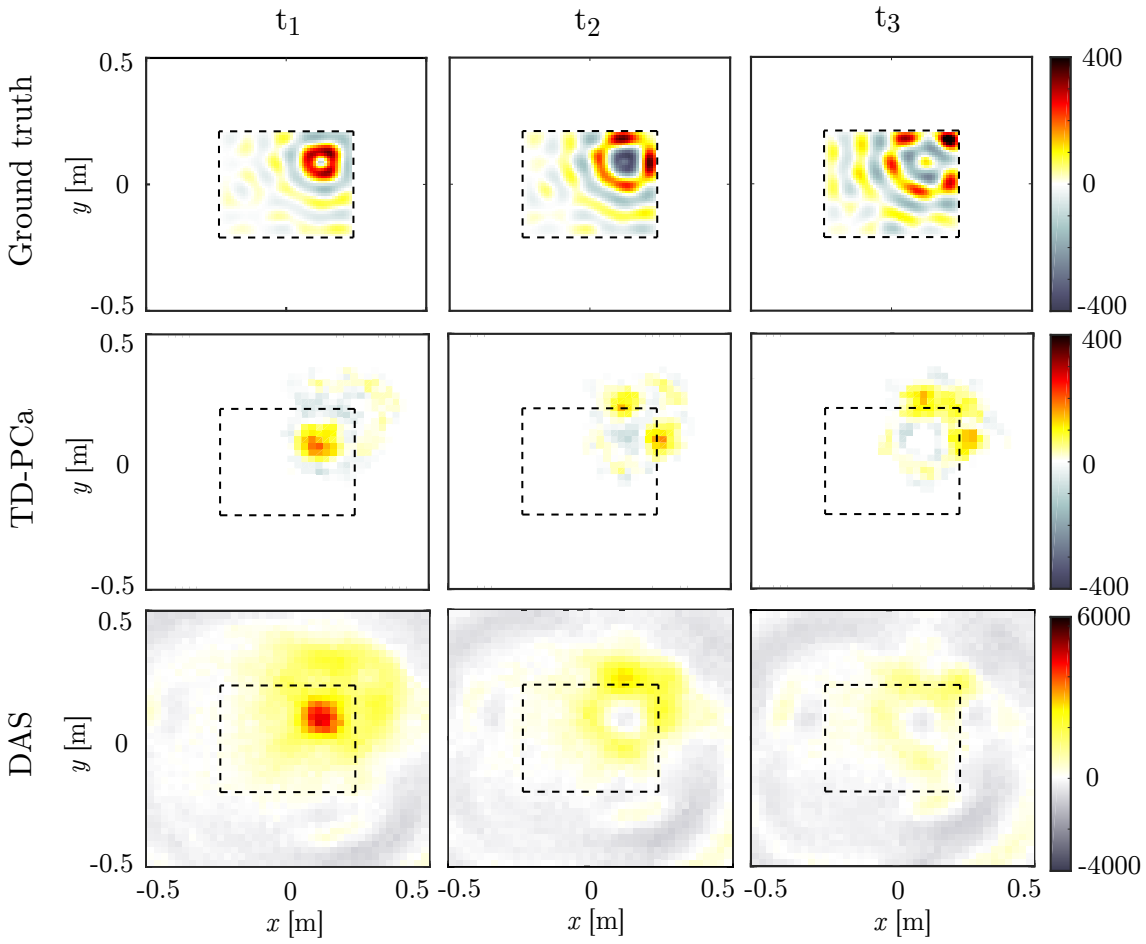

Figure 3: (Top) Simulated acceleration field; (middle) reconstruction using the TD-PCa and (bottom) output of the standard DAS algorithm.

($\Delta t = 1/6400$ s) and the extent of the panel is represented by the dashed line. The first major element to be noted is that the amplitude of the reconstructed acceleration is off by more than a factor 10 when using the DAS since it is based on the unique radiator element hypothesis. On the other hand, TD-PCa is presented on the same color-scale than the simulated acceleration field (ground truth). Indeed, the amplitude of the reconstructed acceleration is pretty similar to the simulated acceleration field, although a little under-determined. Moreover, one can observe that the artefacts in the DAS maps are not present in the TD-PCa images. Indeed, the pixel rejection process has eliminated the majority of the pixels outside the plate. Thus, TD-PCa results in less subjective images than DAS. Also, one can note that the negative wavefront surrounding the impact position in time frame t_1 is recontructed using TD-PCa and that the interactions with the edges of the plate are also reconstructed in time frames t_2 and t_3. From these results, it seems that the TD-PCa can be used for transient vibration field reconstruction without using any a priori information about the source. The following section presents the results obtained for the experimental replicate of the same configuration.

3.2. Experimental Validation

As can be seen in Figure 4, two sets of measurements are conducted. First, deflectometry measurements are performed using a Fastcam Mini AX200 Photron high speed camera (6 400 frames per second) in order to have an experimental acceleration reference measurement [17]. Following this, the microphone array is mounted in front of the panel and the same excitation is used. As a way to have a repeatable excitation, the drop of a pendulum (consisting of a metallic sphere at the end of a nylon string) is triggered using an electromagnet in order to create a point-like impact. The simply-supported conditions of the panel are ensured using a dedicated procedure, as described in [18].

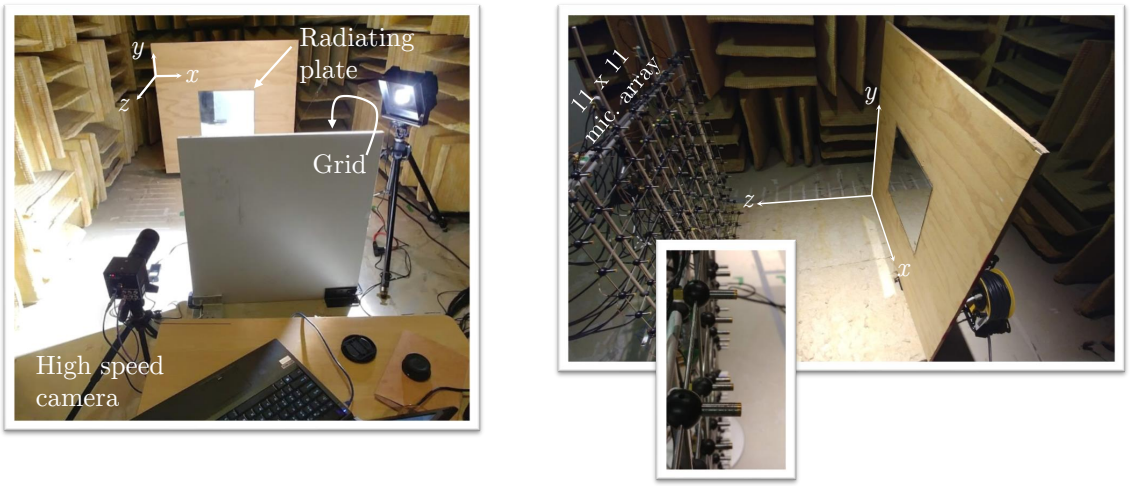

Figure 4: (left) Deflectometry measurement setup and (right) microphone array setup for both measurements.

As for the numerical validation, the imaging results for the deflectometry (ground truth), the TD-PCa acceleration reconstruction and the DAS output are presented in Figure 5 for the three same snapshots as in Section 3.1 (namely: t_1, t_2 and t_3).

Looking at Figure 5, one can see strong similarities with Figure 3. Indeed, the deflectometry measurement for the three snapshots shows that the acceleration source is very similar to the one considered in the simulation. Moreover, the TD-PCa and DAS are practically identical to the results presented in Section 3.1, validating the use of the modal summation method combined with *k-Wave* for the generation, propagation and measurement of the simulated acoustic field. The main difference between the experimental and numerical results lies in the amplitude of the reconstructed acceleration using the TD-PCa. Indeed, it seems that the amplitude is better reconstructed in the experimental case. This probably comes from the fact that the experimental signals measured in anechoic conditions are less noisy than the Signal-to-Noise Ratio (SNR) of 10 dB considered in the simulation. Consequently, the PC maps, although not presented here, are experimentally better resolved (spatially) than numerically. Indeed, this can be seen in the number of pixels conserved in the imaging domain for the TD-PCa reconstruction in Figures 3 and 5. The fact that less pixels are conserved experimentally results in a better conditioned system and in a more representative solution using the Tikhonov regularization.

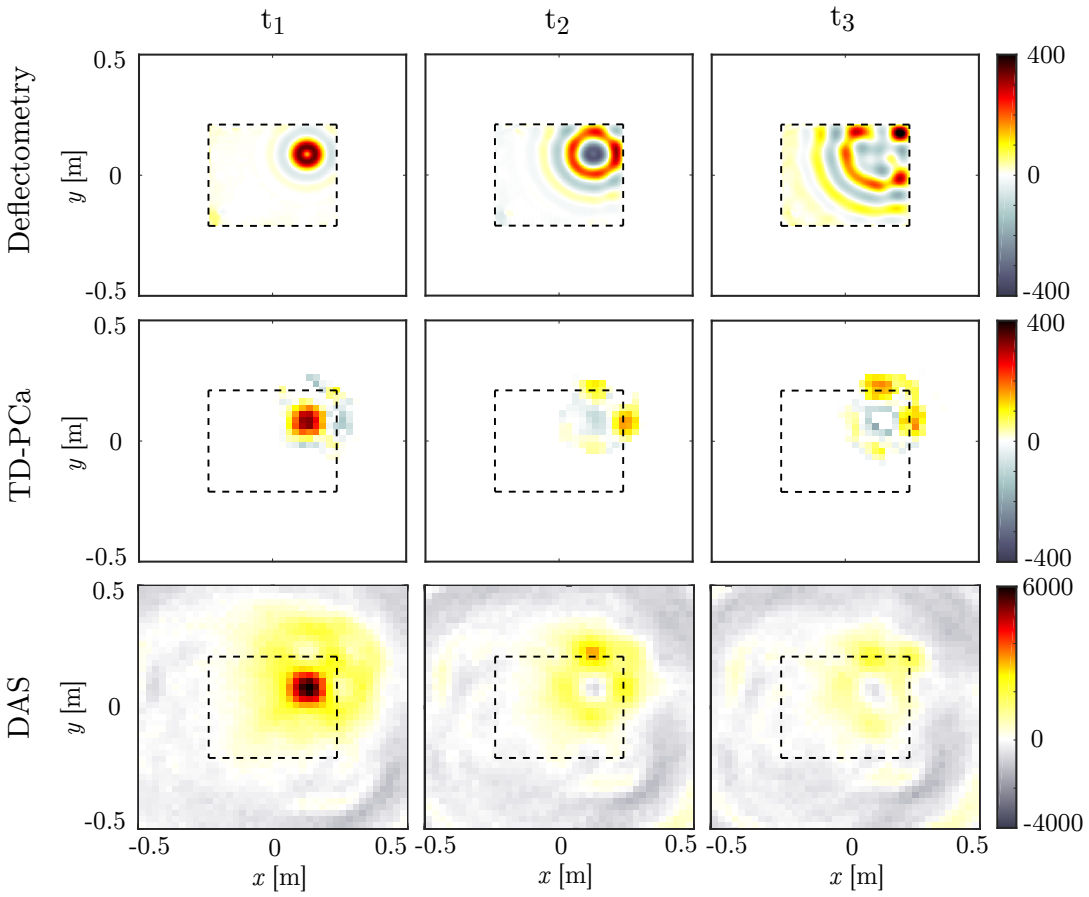

Figure 5: (Top) Deflectometry reconstruction of the normal acceleration; (middle) reconstruction using the TD-PCa and (bottom) output of the standard DAS algorithm.

4. CONCLUSIONS

In this paper, a time-domain imaging algorithm is presented for the acceleration reconstruction of extended transient noise sources. The TD-PCa is based on the phase-coherence principle widely used in image processing and ultrasound imaging. The presented algorithm is divided into two steps: first, using a PC metric, the pixels that are less likely to contribute to the pressure field are rejected from the imaging domain, and second, the Tikhonov regularization is used to solve the inverse formulation of the resulting linear system. An impacted simply-supported baffled panel is considered numerically and experimentally to validate the approach. In both cases, the reconstruction of the transient acceleration field using the TD-PCa is in good agreement with their respective reference. Indeed, TD-PCa allows localizing the position of the impact, imaging the flexural waves around it, capturing some interactions with the edges of the panel and gives a good approximation of the normal acceleration field.

5. ACKNOWLEDGEMENTS

The authors would like to thank the I-INCE for their Young Professional Congress Attendance Grants program and the *Fonds de recherche du Québec - Nature et technologies* (FRQNT) for their funding.

6. REFERENCES

[1] H. Krim and M. Viberg. Two decades of array signal processing research: the parametric approach. *IEEE Signal Processing Magazine*, 13:67–94, 1996.

[2] F. Fahy. *Sound intensity*. London, second edition, 1989.

[3] J. J. Christensen and J. Hald. *Beamforming*. Nærum, 2004.

[4] Q. Leclère, A. Pereira, C. Bailly, J. Antoni, and C. Picard. A unified formalism for acoustic imaging based on microphone array measurements. *International Journal of Aeroacoustics*, 16(4-5):431–456, 2017.

[5] I. Rakotoarisoa, J. Fischer, V. Valeau, D. Marx, C. Prax, and L.-E. Brizzi. Time-domain delay-and-sum beamforming for time-reversal detection of intermittent acoustic sources in flows. *The Journal of the Acoustical Society of America*, 136(5):2675–2686, nov 2014.

[6] J. Fischer, I. Rakotoarisoa, V. Valeau, D. Marx, C. Prax, and L.-E. Brizzi. Time-Domain Imaging Techniques for Aeroacoustic Sources. *Proceedings of the 6th Berlin Beamforming Conference*, pages 1–17, 2016.

[7] Y. Shechtman, Y C. Eldar, O. Cohen, H N. Chapman, J. Miao, and M. Segev. Phase Retrieval with Application to Optical Imaging: A contemporary overview. *IEEE Signal Processing Magazine*, 32(3):87–109, 2015.

[8] J. Camacho and C. Fritsch. Phase Coherence Imaging of Grained Materials. *IEEE Transactions on Ultrasonics, Ferroelectrics, and Frequency Control*, 58(5):1006–1015, 2011.

[9] C. Fritsch, J. Camacho, and M. Parrilla. New ultrasound imaging techniques with phase coherence processing. *Ultrasonics*, 50(2):122–126, 2010.

[10] N. Quaegebeur, T. Padois, P.A. Gauthier, and P. Masson. Enhancement of time-domain acoustic imaging based on generalized cross-correlation and spatial weighting. *Mechanical Systems and Signal Processing*, 75:515–524, 2016.

[11] V. P. Minotto, C. R. Jung, L. G. da Silveira Jr, and B. Lee. GPU-based approaches for real-time sound source localization using the SRP-PHAT algorithm. *International Journal of High Performance Computing Applications*, 2012.

[12] M. Bilodeau, N. Quaegebeur, A. Berry, and P. Masson. Phase coherence imaging of vibroacoustic sources. *Proceedings of the 7th Berlin Beamforming Conference*, pages 1–11, 2018.

[13] X.-Z. Zhang, C.-X. Bi, Y.-B. Zhang, and L Xu. Transient nearfield acoustic holography based on an interpolated time-domain equivalent source method. *The Journal of the Acoustical Society of America*, 130(3):1430–1440, 2011.

[14] P. C. Hansen. Regularization Tools Version 4.0 for Matlab 7.3. *Numerical Algorithms*, 46:189–194, 2007.

[15] A. Putra and D. J. Thompson. Sound radiation from rectangular baffled and unbaffled plates. *Applied Acoustics*, 71(12):1113–1125, 2010.

[16] B. R. Treeby and B. T. Cox. k-Wave: MATLAB toolbox for the simulation and reconstruction of photoacoustic wave-fields. *Journal of Biomedical Optics*, 15(2):021314, 2010.

[17] P. Donoughue, O. Robin, and A. Berry. Measuring the Vibration Response of Plane Panels under Stationary and Transient Mechanical Excitations using Deflectometry. In *Inter-Noise 2016*, pages 615–621, 2016.

[18] O. Robin, J.-D. Chazot, R. Boulandet, M. Michau, A. Berry, and N. Atalla. A Plane and Thin Panel with Representative Simply Supported Boundary Conditions for Laboratory Vibroacoustic Tests. *Acta Acustica united with Acustica*, 102(1):170–182, jan 2016.